Slow photoelectron velocity-map imaging spectroscopy of C_3O^- and C_3S^-

Etienne Garand,[1] Tara I. Yacovitch,[1] and Daniel M. Neumark[1,2,a)]
[1]*Department of Chemistry, University of California, Berkeley, California 94720, USA*
[2]*Chemical Sciences Division, Lawrence Berkeley National Laboratory, Berkeley, California 94720, USA*

(Received 13 May 2009; accepted 14 July 2009; published online 7 August 2009)

High-resolution photodetachment spectra of C_3O^- and C_3S^- using slow photoelectron velocity-map imaging spectroscopy are reported. Well-resolved transitions to the neutral $\tilde{X}\ ^1\Sigma^+$ state are seen for both species. The electron affinities of C_3O and C_3S are determined to be $EA(C_3O) = 1.237 \pm 0.003$ eV and $EA(C_3S) = 1.5957 \pm 0.0010$ eV, respectively. Several vibrational frequencies for gas phase C_3O and C_3S are determined for the first time. The long progression of bending modes observed in the spectra is consistent with electronic structure calculations predicting that the C_3O^- and C_3S^- have bent equilibrium geometries. © *2009 American Institute of Physics*. [DOI: 10.1063/1.3200927]

I. INTRODUCTION

The heteroatom-doped C_nO and C_nS linear carbon chains are important interstellar species. The first three members ($n=1-3$) for each species have been identified in interstellar sources by their rotational spectra.[1–8] In this paper, we continue our investigation of these two isovalent series of clusters via negative ion photodetachment.[9] The high resolution photoelectron (PE) spectra of the C_3O^- and C_3S^- anions are reported, providing a detailed probe of the neutral and anionic ground electronic states of these species.

The C_3O radical has been studied by microwave spectroscopy,[10,11] millimeter-wave spectroscopy,[12] and infrared absorption in rare-gas matrices[13,14] and in the gas phase.[15] Similarly, C_3S has been studied by microwave spectroscopy[6,16,17] and by infrared absorption in rare-gas matrices[18,19] and in the gas phase.[20] Several theoretical studies on the equilibrium geometry, electronic structure, and vibrational spectra of these two species have been reported.[14,21–31] The combination of high-level *ab initio* calculations and microwave spectroscopy of isotopically substituted species has yielded very accurate bond lengths for the neutral C_3O and C_3S.[25,28]

The corresponding C_3O^- and C_3S^- anions have received considerably less attention. The only experimental data on C_3O^- come from the PE spectrum of Oakes and Ellison.[32] This spectrum featured an extended, partially resolved vibrational progression with a frequency of 600 ± 35 cm^{-1}, indicating a large geometry change between the anion and the neutral. The first resolved peak was assigned to the origin transition, yielding an electron affinity (EA) of 1.34 ± 0.15 eV for C_3O. Rienstra-Kiracofe *et al.*[23] subsequently performed electronic structure calculations on C_3O and C_3O^- using the coupled cluster method with single, double, and noniterative triple excitations [CCSD(T)] and found an EA of 0.93 ± 0.10 eV, raising questions about the experimental assignment. No experimental or theoretical studies on the C_3S^- anion have been reported yet.

In this paper, we present high-resolution photodetachment spectra of C_3O^- and C_3S^- using slow photoelectron velocity-map imaging (SEVI). Well-resolved vibrational transitions to the neutral $X\ ^1\Sigma^+$ state are seen for both species. We obtain a revised $EA(C_3O)$ and the first determination of $EA(C_3S)$. The ν_3, ν_4, and ν_5 frequencies for neutral gas phase C_3O and C_3S are also determined. Extended progressions of bending modes observed in the spectra are consistent with both anions having bent equilibrium geometries.

II. EXPERIMENTAL

The SEVI apparatus has been described in detail elsewhere.[33–35] SEVI is a high resolution variant of PE spectroscopy in which mass-selected anions are photodetached at a series of wavelengths. The resulting PEs are collected by velocity-map imaging (VMI) (Ref. 36) using relatively low extraction voltages with the goal of selectively detecting slow electrons with high efficiency and enlarging their image on the detector. At each photodetachment wavelength, one obtains a high resolution PE spectrum over a limited range of electron kinetic energy (eKE).

In this experiment, C_3O^- anions were produced from a gas mixture comprising 1% acetylene and 20% CO_2 in a balance of Ar. Similarly, C_3S^- anions were produced from 1% acetylene and 1% CS_2 in a balance of argon. The gas mixture at a stagnation pressure of 300 psi was expanded into the source vacuum chamber through an Even–Lavie pulsed valve[37] equipped with a grid discharge described in detail elsewhere.[38] Briefly, the gas from the pulsed valve passed through a 2.5×23 mm^2 channel made from Teflon and aluminum within which were two fine grids made of stainless steel wire mesh and separated by 1 mm. The first grid was held to ground while the second was floated to around -500 V_{dc} through a 1 kΩ resistor. The passage of the expanding gas through the grids induced a discharge. Anions formed in the gas expansion were perpendicularly

a)Author to whom correspondence should be addressed. Electronic mail: dneumark@berkeley.edu.

extracted into a Wiley–McLaren[39] time-of-flight mass spectrometer and directed to the detachment region by a series of electrostatic lenses and pinholes. A pulse on the last ion deflector allowed only the desired mass into the interaction region.

Anions were photodetached between the repeller and the extraction plates of the VMI stack by the focused output of a Nd:yttrium aluminum garnet pumped tunable dye laser. The PE cloud formed was then coaxially extracted down a 50 cm flight tube and mapped onto a detector comprising a chevron-mounted pair of time-gated, imaging quality microchannel plates coupled to a phosphor screen, as is typically used in photofragment imaging experiments.[40] Events on the screen were collected by a 1024×1024 charge-coupled device camera and sent to a computer. Electron velocity-mapped images resulting from 50 000–250 000 laser pulses were summed, quadrant symmetrized, and inverse Abel transformed.[41] PE spectra were obtained via angular integration of the transformed images. The spectra presented here are plotted with respect to electron binding energy (eBE), defined as the difference between the energy of the photodetachment photon and the measured eKE.

The apparatus was calibrated by acquiring SEVI images of atomic oxygen[42] at several different photon energies. With the −350 V VMI repeller voltage used in this study, the full widths at half maximum of the oxygen peaks were 7.5 cm^{-1} at 150 cm^{-1} eKE and 18 cm^{-1} at 715 cm^{-1}. In the SEVI experiment, within the same image, all observed transitions have similar widths in pixels (Δr), so transitions observed further from threshold (larger r) are broader in energy. By varying the laser wavelength, a series of images in which the transitions of interest are close to the detachment threshold can be acquired, yielding a complete, high resolution PE spectrum.

SEVI also provides information on the photoelectron angular distribution (PAD). For one-photon detachment, the PAD is given by[43,44]

$$\frac{d\sigma}{d\Omega}=\frac{\sigma_{\mathrm{tot}}}{4\pi}\left(1+\beta\left(\tfrac{3}{2}\cos^2(\theta)-\tfrac{1}{2}\right)\right), \quad (1)$$

where θ is the angle between the direction of the PE ejection and the polarization vector of the incident photon. The anisotropy parameter β lies between 2 and −1 and provides information on the orbital angular momentum (l) of the ejected PE; $l=0$ (s-wave) detachment leads to $\beta=0$, $l=1$ (p-wave) to $\beta=2$ and $l=0$ and 2 with equal amplitude and phase ($s+d$ wave) to $\beta=-1$.

III. RESULTS

The transformed SEVI images of C_3O^- and C_3S^- taken at photon energies of 14 493 and 15 037 cm^{-1}, respectively, are presented in Fig. 1. Both images display a similar series of closely spaced doublets. However, the two images display features with different PADs, as seen most clearly on the outermost rings. In the C_3O^- image, these rings have more intensity in the direction parallel to the laser electric field, corresponding to $\beta>0$. In contrast, features in the C_3S^- images are more intense in the direction perpendicular to the electric field, indicating $\beta<0$. Figure 2 shows the β values for the main features in the SEVI images shown in Fig. 1 as a function of their eKE. The highest energy features (outermost ring) have $\beta=0.6\pm0.1$ and $\beta=-0.8\pm0.1$ for C_3O^- and C_3S^-, respectively. In both images, the rings become more isotropic ($\beta=0$) with decreasing radius, consistent with our expectation that s-wave detachment, when allowed, dominates near threshold.[34,45]

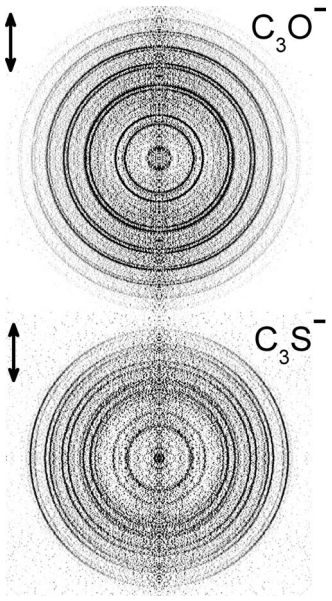

FIG. 1. Inverse-Abel transformed SEVI images of C_3O^- (top) and C_3S^- (bottom) taken at photon energies of 14 493 and 15 037 cm^{-1}, respectively. Arrows indicate the polarization vector of the laser.

PE spectra obtained from the C_3O^- and C_3S^- SEVI images are shown in Figs. 3 and 4. Each spectrum is composed of several SEVI traces taken at different photon energies and joined together. The C_3O^- spectrum comprises an extended progression of multiplets spread over more than 7000 cm^{-1}. Its most prominent attribute is the progression of peaks labeled A_n, spaced by an average of 603 cm^{-1}. The peak with maximum intensity is A_8, which is located 4801 cm^{-1} above

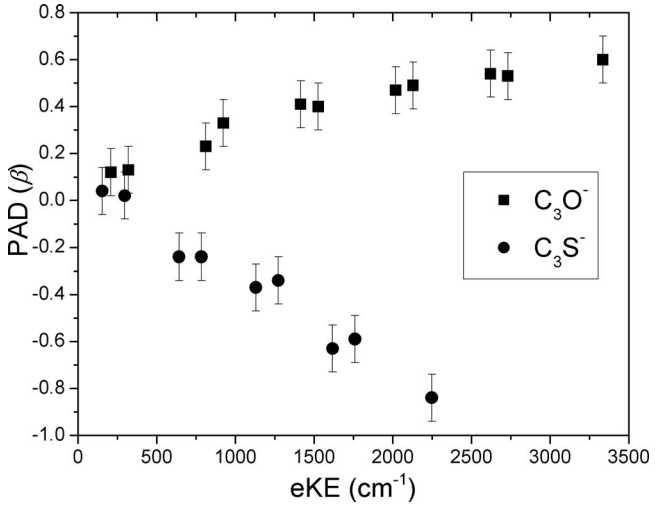

FIG. 2. Anisotropy parameters β [Eq. (1)] for the main features in the C_3O^- (squares) and C_3S^- (circles) images shown in Fig. 1 as a function of their eKE.

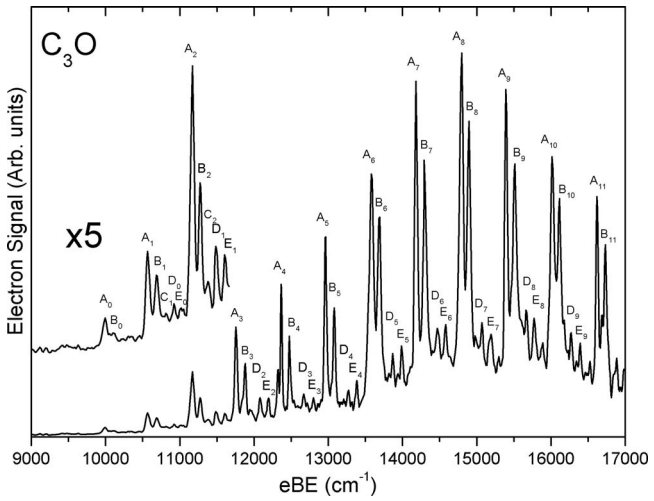

FIG. 3. SEVI spectra of C_3O^- covering the eBE range of 9000–17 000 cm^{-1}.

A_0. A second, slightly less intense progression B_n has a similar spacing; each peak B_n lies 111 cm^{-1} above the corresponding A_n peak on average. The SEVI spectrum shows considerably more structure than the lower resolution PE spectra of Oakes and Ellison,[32] in which only a single, partially resolved progression of peaks spaced by 600 cm^{-1} was observed, with no evidence for the multiplet structure seen here.

The C_3S^- spectrum displays a similar pattern. There are two clear progressions, A_n and B_n. The progression A_n has a characteristic spacing of 488 cm^{-1} and each peak B_n appears, on average, 142 cm^{-1} above the corresponding peak A_n. The A_n and B_n progressions are less extended than in C_3O^-, and the most intense feature in the C_3S^- spectrum (B_3) is found 1583 cm^{-1} above A_0. In both spectra, lower intensity peaks labeled C_n, D_n, and E_n are also resolved between the main transitions. Peak positions in the C_3O^- and C_3S^- SEVI spectra are presented in Tables I and II.

IV. ELECTRONIC STRUCTURE CALCULATIONS

Electronic structure calculations were performed on the relevant neutral and anionic states of C_3O and C_3S to produce at a uniform level of theory all the geometries and vibrational frequencies necessary to interpret the PE spectra. Our calculations were carried out with density functional theory (DFT) using the Becke three-parameter Lee, Yang, and Parr (B3LYP) exchange-correlation functional[46,47] and the augmented correlation consistent polarized valence triple-zeta (AVTZ) basis set.[48] All computations were performed using the GAUSSIAN03 program.[49]

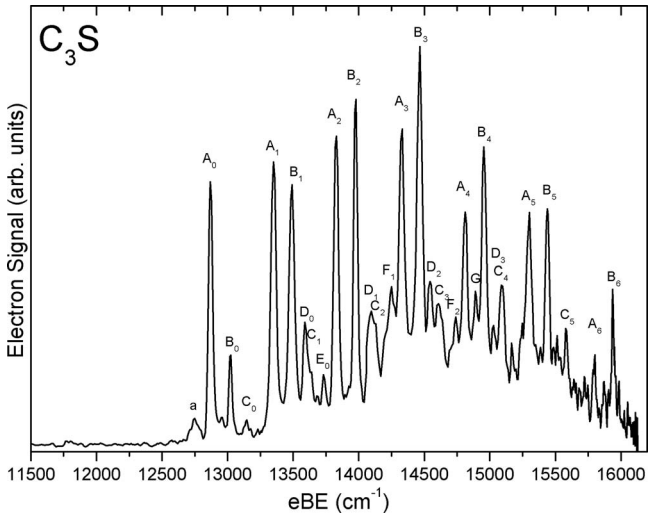

FIG. 4. SEVI spectra of C_3S^- covering the eBE range of 11 500–16 250 cm^{-1}.

TABLE I. Peak positions, shifts from origin, and assignments for the C_3O^- SEVI spectra.

Peak label	Position (cm^{-1})	Shift (cm^{-1})	Assignment
A_0	9 988	0	0_0^0
B_0	10 097	109	5_0^1
A_1	10 569	581	4_0^1
B_1	10 692	704	$4_0^1 5_0^1$
C_1	10 813	825	$4_0^1 5_0^2$
D_0	10 923	935	3_0^1
E_0	11 029	1041	$3_0^1 5_0^1$
A_2	11 169	1181	4_0^2
B_2	11 273	1285	$4_0^2 5_0^1$
C_2	11 375	1387	$4_0^2 5_0^2$
D_1	11 495	1507	$3_0^1 4_0^1$
E_1	11 612	1624	$3_0^1 4_0^1 5_0^1$
A_3	11 758	1770	4_0^3
B_3	11 879	1891	$4_0^3 5_0^1$
D_2	12 083	2095	$3_0^1 4_0^2$
E_2	12 195	2207	$3_0^1 4_0^2 5_0^1$
A_4	12 366	2378	4_0^4
B_4	12 475	2487	$4_0^4 5_0^1$
D_3	12 668	2680	$3_0^1 4_0^3$
E_3	12 802	2814	$3_0^1 4_0^3 5_0^1$
A_5	12 962	2974	4_0^5
B_5	13 081	3093	$4_0^5 5_0^1$
D_4	13 270	3282	$3_0^1 4_0^4$
E_4	13 383	3395	$3_0^1 4_0^4 5_0^1$
A_6	13 582	3594	4_0^6
B_6	13 687	3699	$4_0^6 5_0^1$
D_5	13 868	3880	$3_0^1 4_0^5$
E_5	13 991	4003	$3_0^1 4_0^5 5_0^1$
A_7	14 183	4195	4_0^7
B_7	14 294	4306	$4_0^7 5_0^1$
D_6	14 473	4485	$3_0^1 4_0^6$
E_6	14 591	4603	$3_0^1 4_0^2 5_0^1$
A_8	14 789	4801	4_0^8
B_8	14 898	4910	$4_0^8 5_0^1$
D_7	15 068	5080	$3_0^1 4_0^7$
E_7	15 186	5198	$3_0^1 4_0^2 5_0^1$
A_9	15 395	5407	4_0^9
B_9	15 505	5517	$4_0^9 5_0^1$
D_8	15 677	5689	$3_0^1 4_0^8$
E_8	15 780	5792	$3_0^1 4_0^2 5_0^1$
A_{10}	16 008	6020	4_0^{10}
B_{10}	16 112	6124	$4_0^{10} 5_0^1$
D_9	16 280	6292	$3_0^1 4_0^9$
E_9	16 393	6405	$3_0^1 4_0^2 5_0^1$
A_{11}	16 621	6633	4_0^{11}
B_{11}	16 726	6738	$4_0^{11} 5_0^1$

The calculated geometries and relative energies of the different states are shown in Table III while the harmonic

TABLE II. Peak positions, shifts from origin, and assignments for the C_3S^- SEVI spectra.

Peak label	Position (cm^{-1})	Shift (cm^{-1})	Assignment
A	12 752	−118	4_1^0
A_0	12 870	0	0_0^0
B_0	13 021	151	5_0^1
C_0	13 142	272	5_0^2
A_1	13 348	478	4_0^1
B_1	13 490	621	$4_0^1 5_0^1$
D_0	13 591	721	3_0^1
C_1	13 633	763	$4_0^1 5_0^2$
E_0	13 735	865	$3_0^1 5_0^1$
A_2	13 829	959	4_0^2
B_2	13 976	1106	$4_0^2 5_0^1$
D_1	14 073	1203	$3_0^1 4_0^1$
C_2	14 116	1246	$4_0^2 5_0^2$
F_0	14 252	1382	3_0^2
A_3	14 319	1449	4_0^3
B_3	14 453	1583	$4_0^3 5_0^1$
D_2	14 532	1662	$3_0^1 4_0^2$
C_3	14 599	1729	$4_0^3 5_0^2$
F_1	14 740	1870	$3_0^2 4_0^1$
A_4	14 811	1941	4_0^4
G	14 891	2021	$3_0^2 4_0^1 5_0^1$
B_4	14 955	2085	$4_0^4 5_0^1$
D_3	15 026	2156	$3_0^1 4_0^3$
C_4	15 092	2222	$4_0^4 5_0^2$
A_5	15 298	2428	4_0^5
B_5	15 438	2568	$4_0^5 5_0^1$
C_5	15 581	2712	$4_0^5 5_0^2$
A_6	15 797	2927	4_0^6
B_6	15 939	3069	$4_0^6 5_0^1$

vibrational frequencies are presented in Table IV. The bond lengths of the neutral $^1\Sigma^+$ ground state of C_3O and C_3S calculated here are all found to lie within 0.007 Å of the recommended values[25,28] for these species. Both neutral species show a short C_1C_2 bond and a longer C_2C_3 bond. For the C_3O^- and C_3S^- anions, we found a bent $^2A'$ ground state. In both species, the $^2\Pi$ linear geometry is found to be a first-order transition state between the two equivalent bent structures. For C_3O^-, the bent minimum is found to be 0.17 eV below the linear geometry. The $^2A'$ state has a C_2C_3O angle of 142.5° and a $C_1C_2C_3$ angle of 167.8°. This geometry is very similar to the higher level CCSD(T)/AVTZ result of Rienstra-Kiracofe *et al.*[23] In C_3S^-, the bent minimum is only 0.02 eV below the linear geometry; the C_2C_3S angle is 171.0° and the $C_1C_2C_3$ angle is 177.7°. For C_3S^-, we found very similar lengths for the two CC bonds and a slightly longer CS bond than in the corresponding neutral. In contrast, for C_3O^- we found a short C_1C_2 bond, a long C_2C_3 bond, and a longer CO bond.

V. ANALYSIS AND DISCUSSION

In this section, we present a detailed assignment of the features observed in the SEVI spectra. In addition to the calculations presented here, the neutral C_3O and C_3S vibrational frequencies observed in argon matrix isolation experiments[14,18] and the anharmonic frequency calculations of Hochlaf and co-workers[24,31] are used as guidelines for the assignments. The peak assignments are summarized in Tables I and II.

For both species, the main progression labeled A_n is assigned to 4_0^n transitions involving the C_2C_3X bending vibration. In C_3O, the position of the 4_0^1 transition (peak A_1) yields 581 cm^{-1} for the υ_4 fundamental in excellent agreement with the value of 580.0 cm^{-1} measured in an argon matrix[14] and the calculated value[24] of 584.4 cm^{-1}. Similarly, the υ_4 fundamental in C_3S is found to be 478 cm^{-1}. Our spectra represent the first experimental observation of this mode in C_3S but its frequency is in excellent agreement with the calculated value[31] of 475.8 cm^{-1}. The peaks labeled B_n are assigned to the $4_0^n 5_0^1$ combination bands. The υ_5 mode corresponds to the low-frequency $C_1C_2C_3$ carbon chain bending mode. The position of peak B_0 yields υ_5 fundamentals of 109 and 151 cm^{-1} for C_3O and C_3S, respectively; both values are the first direct experimental observation of these modes. Our υ_5 frequency for C_3O is in good agreement with the value of 120 cm^{-1} estimated by Botschwina and Reisenauer[14] from *l*-type doubling and rotational constants. The calculated υ_5 frequencies[24,31] of 114.0 and 145.0 cm^{-1} for C_3O and C_3S, respectively, are again in excellent agreement with the value found here. The spacing between peaks

TABLE III. Calculated relative energies and geometries at the B3LYP/AVTZ level of theory. All bond lengths are in angstrom. The recommended bond length values for the neutral $^1\Sigma^+$ C_3O (Ref. 28) and $^1\Sigma^+$ C_3S (Ref. 25) are shown in parentheses.

	State	ΔE (eV)	$R(C_1C_2)$	$R(C_2C_3)$	$R(C_3X)$	$\theta(C_1C_2C_3)$	$\theta(C_2C_3X)$	$\theta(C_1C_2C_3X)$
C_3O								
Anion	$^2A'$	0.0	1.261	1.357	1.210	167.8	142.5	180
	$^2\Pi$ [a]	0.17	1.296	1.290	1.207	180	180	···
Neutral	$^1\Sigma^+$	1.21	1.266 (1.2728)	1.294 (1.2971)	1.149 (1.1485)	180	180	···
C_3S								
Anion	$^2A'$	0.0	1.286	1.296	1.606	177.7	171.0	180
	$^2\Pi$ [a]	0.02	1.287	1.293	1.605	180	180	···
Neutral	$^1\Sigma^+$	1.73	1.274 (1.2810)	1.289 (1.2927)	1.542 (1.5374)	180	180	···

[a]First-order transition state.

TABLE IV. Calculated harmonic frequencies (cm^{-1}) at the B3LYP/AVTZ level of theory.

		υ_1	υ_2	υ_3	υ_4	υ_5
	State	CCC asymmetric stretch	CCX asymmetric stretch	CCCX symmetric stretch	CCX bend	CCC bend
C_3O						
Anion	$^2A'$	1936	1766	915	527	239/226
	$^2\Pi$ [a]	2084	1622	923	609/324*i*	285/203
Neutral	$^1\Sigma^+$	2329	1975	966	602	142
C_3S						
Anion	$^2A'$	1840	1440	670	52	360/270
	$^2\Pi$ [a]	1842	1443	669	511/38*i*	354/191
Neutral	$^1\Sigma^+$	2136	1566	739	498	161

[a]First-order transition state.

A_n and C_n is found to be about twice the A_n-B_n splitting and thus the C_n peaks are assigned to the $4_0^n5_0^2$ transitions.

In the spectra of both species, the spacing in the less intense progression labeled D_n is similar to the υ_4 frequency and the first peak D_0 appears only after peak A_1. The D_n progression is thus assigned to the $3_0^14_0^n$ transitions. The υ_3 mode is the symmetric stretch of the three bonds. The position of peak D_0 yields a υ_3 fundamental of 935 and 721 cm^{-1} for C_3O and C_3S, respectively. This assignment is consistent with the values of 939.1 and 725.6 cm^{-1} found for C_3O and C_3S, respectively, in argon matrix isolation experiments.[14,18] The D_n-E_n spacing is similar to the υ_5 frequency and thus the E_n peaks are assigned to the $3_0^14_0^n5_0^1$ transitions. A few extra peaks are found in the C_3S^- spectra. The peaks labeled F_n are assigned to the $3_0^24_0^n$ transitions while peak G is assigned to the $3_0^24_0^15_0^1$ transition. The small peak labeled A is found 118 cm^{-1} below the origin transition and is assigned to a hot band transition. The most likely excited vibration in C_3S^- is the υ_4 mode for which the calculated frequency is only 52 cm^{-1}. Peak A is thus assigned to the 4_1^0 transition, yielding a 118 cm^{-1} frequency for this mode in the anion. The difference between the experimental and calculated frequencies reflects the sensitivity of this mode to the height of the small barrier to linearity.

For both species, the position of peak A_0 yields the adiabatic EA. These values are determined as $EA(C_3O) = 1.237 \pm 0.003$ eV and $EA(C_3S) = 1.5957 \pm 0.0010$ eV. The uncertainty on the EA of C_3O is slightly larger than on C_3S because the very weak intensity of the origin peak in C_3O prevented us from acquiring a spectrum at photon energy close to the detachment threshold. The EA of C_3O found here is within the large error bars of the previous value of 1.34 ± 0.15 eV, but the feature assigned as the band origin by Oakes and Ellison[32] corresponds to the A_1/B_1 doublet of the SEVI spectra. The revised $EA(C_3O)$ is in excellent agreement with the value of 1.21 eV B3LYP/AVTZ calculated here but is still ~0.3 eV larger than the value of 0.93 ± 0.10 eV calculated by Rienstra-Kiracofe *et al.*[23] at the higher CCSD(T)/AVTZ level of theory. The experimental EA of C_3S is reported for the first time and is found to be slightly smaller than the value of 1.73 eV calculated at the B3LYP/AVTZ level. The electron affinities and vibrational frequencies determined in this study are summarized in Table V.

The SEVI spectra of C_3O^- and C_3S^- exhibit substantial bending activity, as expected for photodetachment from bent anions to linear neutral states. The longer ν_4 progression in the C_3O^- spectrum is consistent with our calculations indicating that this anion is considerably more bent than C_3S^-. However, even the relatively small deviation from linearity in the calculated C_3S^- geometry is sufficient to induce substantial bend progressions in the SEVI spectrum. In order to understand these effects in more detail, we attempted to simulate the spectra for both species with the usual Franck–Condon and harmonic approximations.[50,51] The C_3O^- and C_3S^- simulated spectra are shown in the middle panels of Figs. 5 and 6, respectively. Neither spectrum could be simulated very well by using the *ab initio* geometries and frequencies. The C_3O simulation displays too much activity in the υ_4 mode and not enough in the υ_3 mode. On the other hand, the C_3S simulation does not display enough activity in the υ_4 and υ_3 modes. In other to get reasonable agreement with the experimental spectra, the normal mode displacements of all the active modes need to be adjusted with the υ_4 mode requiring the larger adjustments. The results of the simulations with optimized parameters are shown in the bottom panel of Figs. 5 and 6. The optimized parameters correspond to anion structures with $\theta(C_1C_2C_3) = 172°$ and $\theta(C_2C_3O) = 148°$ for C_3O^- and $\theta(C_1C_2C_3) = 175°$ and $\theta(C_2C_3S) = 160°$ for C_3S^-. It thus appears that our electronic structure calculations overestimate the distortion from linearity in C_3O^- and underestimate it in C_3S^-. However, we should point out that the analysis used here neglects effects from large-amplitude bending motion and Renner–Teller

TABLE V. Experimentally determined adiabatic EAs and fundamental vibrational frequencies for C_3O and C_3S. Error bars on vibrational frequencies are ± 8 cm^{-1}.

	EA (eV)	υ_3 (cm^{-1})	υ_4 (cm^{-1})	υ_5 (cm^{-1})
C_3O	1.237 ± 0.003	935	581	109
C_3S	1.5957 ± 0.0010	721	478	151

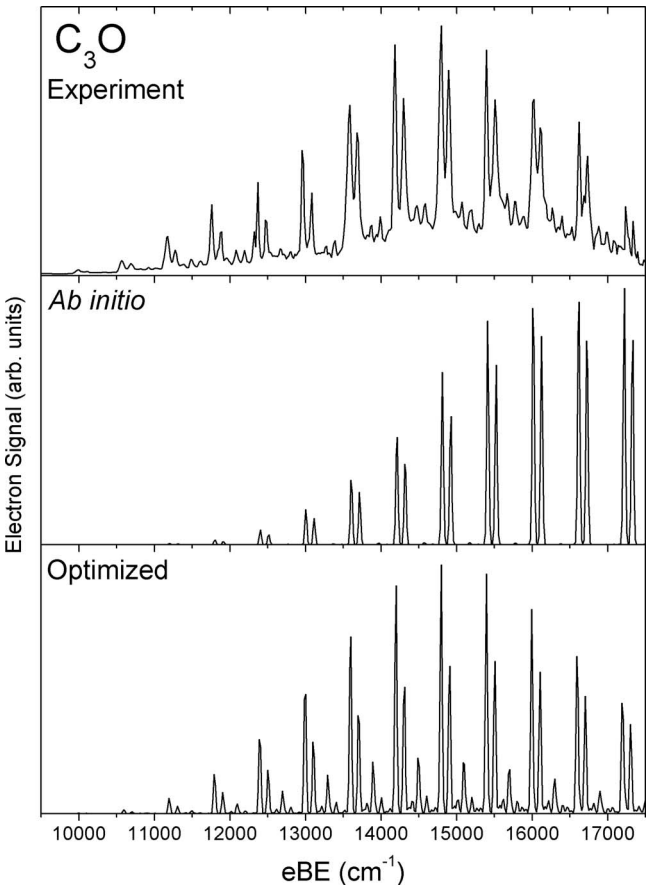

FIG. 5. Franck–Condon simulation of the C_3O^- SEVI spectra using *ab initio* (center) and optimized (lower panel) parameters. Experimental spectrum is shown in top panel for comparison.

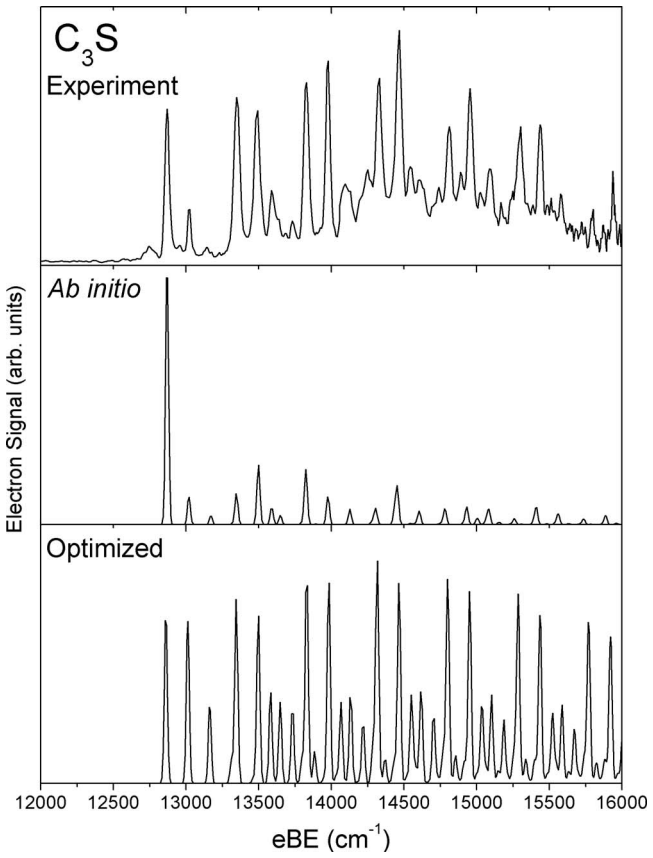

FIG. 6. Franck–Condon simulation of the C_3S^- SEVI spectra using *ab initio* (center) and optimized (lower panel) parameters. Experimental spectrum is shown in top panel for comparison.

coupling in the anions, so the optimized geometries are only approximate.

The last point to discuss is the different PE angular distributions in the C_3O^- and C_3S^- SEVI spectra, as shown in Fig. 2. Close to the detachment threshold, *s*-wave detachment should dominate for both species,[45] consistent with the nearly isotropic PADs observed here, and the contributions from higher partial waves should grow with increasing eKE. We indeed see increasingly anisotropic PADs, but while the features in the C_3O^- spectra exhibit *p*-wave character, those in the C_3S^- spectra show $s+d$ wave character. In both cases, the electron is ejected from an a' orbital with significant amplitude on all four atoms; detachment via *s*, *p*, and *d* partial waves is allowed. However, C_3S^- is nearly linear, and the molecular orbital from which detachment occurs is similar to a π-orbital in a linear molecule. Even though all partial waves are allowed by symmetry from such an orbital, in practice $s+d$ wave detachment is often dominant.[9,52] In a more strongly bent species such as C_3O^-, the propensity rules for detachment are expected to be less strict, so one might expect *p*-wave detachment to become increasingly more important at higher eKE. The C_3O^- and C_3S^- PADs thus most likely reflect the difference in geometry between the two anions predicted by our DFT calculations.

VI. CONCLUSIONS

High resolution PE spectra of C_3O^- and C_3S^- obtained using SEVI are reported. These spectra provide a more accurate EA of 1.237 ± 0.003 eV for C_3O and the first measured EA of 1.5957 ± 0.0010 eV for C_3S. In addition, we determine the gas-phase vibrational frequencies of the υ_3, υ_4, and υ_5 modes for neutral C_3O and C_3S in their $\tilde{X}\ ^1\Sigma^+$ ground states. Since the neutral species are linear, extended progressions of bending modes in the SEVI spectra are consistent with bent equilibrium geometries for both the C_3O^- and C_3S^- anions.

ACKNOWLEDGMENTS

This work was supported by the Air Force Office of Scientific Research under Grant No. F49620-03-1-0085. E.G. thanks the National Science and Engineering Research Council of Canada (NSERC) for a postgraduate scholarship and T.Y. thanks the Fonds Québécois de la Recherche sur la Nature et les Technologies (FQRNT) for a master's scholarship.

[1] A. A. Penzias, P. M. Solomon, R. W. Wilson, and K. B. Jefferts, Astrophys. J. **168**, L53 (1971).
[2] A. M. Smith and T. P. Stecher, Astrophys. J. **164**, L43 (1971).
[3] P. Solomon, K. B. Jefferts, A. A. Penzias, and R. W. Wilson, Astrophys. J. **163**, L53 (1971).
[4] H. E. Matthews, W. M. Irvine, P. Friberg, R. D. Brown, and P. D. Godfrey, Nature (London) **310**, 125 (1984).
[5] R. D. Brown, P. D. Godfrey, D. M. Cragg, E. H. N. Rice, W. M. Irvine, P. Friberg, H. Suzuki, M. Ohishi, N. Kaifu, and M. Morimoto, Astrophys. J. **297**, 302 (1985).
[6] S. Yamamoto, S. Saito, K. Kawaguchi, N. Kaifu, H. Suzuki, and M. Ohishi, Astrophys. J. **317**, L119 (1987).

[7] S. Saito, K. Kawaguchi, S. Yamamoto, M. Ohishi, H. Suzuki, and N. Kaifu, Astrophys. J. **317**, L115 (1987).
[8] M. Ohishi, H. Suzuki, S. I. Ishikawa, C. Yamada, H. Kanamori, W. M. Irvine, R. D. Brown, P. D. Godfrey, and N. Kaifu, Astrophys. J. **380**, L39 (1991).
[9] E. Garand, T. I. Yacovitch, and D. M. Neumark, J. Chem. Phys. **129**, 074312 (2008).
[10] R. D. Brown, P. D. Godfrey, P. S. Elmes, M. Rodler, and L. M. Tack, J. Am. Chem. Soc. **107**, 4112 (1985).
[11] T. B. Tang, H. Inokuchi, S. Saito, C. Yamada, and E. Hirota, Chem. Phys. Lett. **116**, 83 (1985).
[12] W. Klebsch, M. Bester, K. M. T. Yamada, G. Winnewisser, W. Joentgen, H. J. Altenbach, and E. Vogel, Astron. Astrophys. **152**, L12 (1985).
[13] R. L. Dekock and W. Weltner, J. Am. Chem. Soc. **93**, 7106 (1971).
[14] P. Botschwina and H. P. Reisenauer, Chem. Phys. Lett. **183**, 217 (1991).
[15] D. McNaughton, D. McGilvery, and F. Shanks, J. Mol. Spectrosc. **149**, 458 (1991).
[16] Y. Ohshima and Y. Endo, J. Mol. Spectrosc. **153**, 627 (1992).
[17] J. A. Tang and S. Saito, J. Mol. Spectrosc. **169**, 92 (1995).
[18] G. Maier, J. Schrot, H. P. Reisenauer, and R. Janoschek, Chem. Ber. **124**, 2617 (1991).
[19] J. Szczepanski, R. Hodyss, J. Fuller, and M. Vala, J. Phys. Chem. A **103**, 2975 (1999).
[20] S. Takano, J. Tang, and S. Saito, J. Mol. Spectrosc. **178**, 194 (1996).
[21] R. D. Suenram and F. J. Lovas, Astrophys. J. **429**, L89 (1994).
[22] G. Pascoli and H. Lavendy, Int. J. Mass. Spectrom. **181**, 11 (1998).
[23] J. C. Rienstra-Kiracofe, G. B. Ellison, B. C. Hoffman, and H. F. Schaefer, J. Phys. Chem. A **104**, 2273 (2000).
[24] M. Hochlaf, J. Mol. Spectrosc. **210**, 284 (2001).
[25] P. Botschwina, Phys. Chem. Chem. Phys. **5**, 3337 (2003).
[26] G. L. Li and Z. C. Tang, J. Phys. Chem. A **107**, 5317 (2003).
[27] I. Perez-Juste, A. M. Grana, L. Carballeira, and R. A. Mosquera, J. Chem. Phys. **121**, 10447 (2004).
[28] P. Botschwina, J. Mol. Struct.: THEOCHEM **724**, 95 (2005).
[29] H. Wang, J. Szczepanski, P. Brucat, and M. Vala, Int. J. Quantum Chem. **102**, 795 (2005).
[30] H. Y. Wang, J. Szczepanski, A. Cooke, P. Brucat, and M. Vala, Int. J. Quantum Chem. **102**, 806 (2005).
[31] A. Zaidi, S. Lahmar, Z. Ben Lakhdar, P. Rosmus, and M. Hochlaf, Theor. Chem. Acc. **114**, 341 (2005).
[32] J. M. Oakes and G. B. Ellison, Tetrahedron **42**, 6263 (1986).
[33] A. Osterwalder, M. J. Nee, J. Zhou, and D. M. Neumark, J. Chem. Phys. **121**, 6317 (2004).
[34] M. J. Nee, A. Osterwalder, J. Zhou, and D. M. Neumark, J. Chem. Phys. **125**, 014306 (2006).
[35] D. M. Neumark, J. Phys. Chem. A **112**, 13287 (2008).
[36] A. Eppink and D. H. Parker, Rev. Sci. Instrum. **68**, 3477 (1997).
[37] U. Even, J. Jortner, D. Noy, N. Lavie, and C. Cossart-Magos, J. Chem. Phys. **112**, 8068 (2000).
[38] E. Garand, T. I. Yacovitch, and D. M. Neumark, J. Chem. Phys. **130**, 064304 (2009).
[39] W. C. Wiley and I. H. McLaren, Rev. Sci. Instrum. **26**, 1150 (1955).
[40] D. W. Chandler and P. L. Houston, J. Chem. Phys. **87**, 1445 (1987).
[41] E. W. Hansen and P. L. Law, J. Opt. Soc. Am. A **2**, 510 (1985).
[42] D. M. Neumark, K. R. Lykke, T. Andersen, and W. C. Lineberger, Phys. Rev. A **32**, 1890 (1985).
[43] J. Cooper and R. N. Zare, J. Chem. Phys. **48**, 942 (1968).
[44] K. L. Reid, Annu. Rev. Phys. Chem. **54**, 397 (2003).
[45] E. P. Wigner, Phys. Rev. **73**, 1002 (1948).
[46] A. D. Becke, J. Chem. Phys. **98**, 1372 (1993).
[47] C. T. Lee, W. T. Yang, and R. G. Parr, Phys. Rev. B **37**, 785 (1988).
[48] T. H. Dunning, J. Chem. Phys. **90**, 1007 (1989).
[49] M. J. Frisch, G. W. Trucks, H. B. Schlegel *et al.*, GAUSSIAN03, Revision C.02, Gaussian, Inc., Wallingford, CT, 2004.
[50] P. Chen, in *Unimolecular and Bimolecular Reaction Dynamics*, edited by T. Baer, C.-Y. Ng, and I. Powis (Wiley, New York, 1994), p. 371.
[51] E. H. Kim, S. E. Bradforth, D. W. Arnold, R. B. Metz, and D. M. Neumark, J. Chem. Phys. **103**, 7801 (1995).
[52] T. R. Taylor, C. S. Xu, and D. M. Neumark, J. Chem. Phys. **108**, 10018 (1998).